Molecular Cell
Article

The ClpS Adaptor Mediates Staged Delivery of N-End Rule Substrates to the AAA+ ClpAP Protease

Giselle Román-Hernández,[1] Jennifer Y. Hou,[1] Robert A. Grant,[1] Robert T. Sauer,[1] and Tania A. Baker[1,2,*]
[1]Department of Biology
[2]Howard Hughes Medical Institute
Massachusetts Institute of Technology, Cambridge, MA 02139, USA
*Correspondence: tabaker@mit.edu
DOI 10.1016/j.molcel.2011.06.009

SUMMARY

The ClpS adaptor delivers N-end rule substrates to ClpAP, an energy-dependent AAA+ protease, for degradation. How ClpS binds specific N-end residues is known in atomic detail and clarified here, but the delivery mechanism is poorly understood. We show that substrate binding is enhanced when ClpS binds hexameric ClpA. Reciprocally, N-end rule substrates increase ClpS affinity for $ClpA_6$. Enhanced binding requires the N-end residue and a peptide bond of the substrate, as well as multiple aspects of ClpS, including a side chain that contacts the substrate α-amino group and the flexible N-terminal extension (NTE). Finally, enhancement also needs the N domain and AAA+ rings of ClpA, connected by a long linker. The NTE can be engaged by the ClpA translocation pore, but ClpS resists unfolding/degradation. We propose a staged-delivery model that illustrates how intimate contacts between the substrate, adaptor, and protease reprogram specificity and coordinate handoff from the adaptor to the protease.

INTRODUCTION

The N-end rule relates degradation susceptibility to a protein's N-terminal amino acid (Bachmair et al., 1986; Varshavsky, 2008). In bacteria, four N-terminal residues (Tyr, Phe, Trp, and Leu) serve as primary N-end degrons (Tobias et al., 1991). The ClpS adaptor binds these residues and delivers attached substrates to the AAA+ ClpAP protease for degradation (Erbse et al., 2006; Wang et al., 2007). In eukaryotes, a family of E3 ubiquitin ligases with a small region homologous to ClpS recognizes and covalently modifies N-end rule substrates with polyubiquitin, targeting these modified proteins to the proteasome (Lupas and Koretke, 2003; Tasaki and Kwon, 2007).

ClpAP, one of five degradation machines in *Escherichia coli*, consists of the $ClpP_{14}$ protease and the $ClpA_6$ unfoldase. $ClpA_6$ is active as a hexamer composed of two AAA+ rings (D1 and D2) and also carries a family-specific N domain, which is flexibly attached to the D1 ring (Gottesman and Maurizi, 1992; Cranz-Mileva et al., 2008; Effantin et al., 2010). Using the energy of ATP binding and hydrolysis, machinery in the axial pore of $ClpA_6$ unfolds and translocates protein substrates through this pore and into the $ClpP_{14}$ chamber (Figure 1A; Hinnerwisch et al., 2005; Kress et al., 2009).

E. coli ClpS has a folded core domain (residues 26–106) and a poorly structured N-terminal extension (NTE; residues 1–25; Figure 1B; Zeth et al., 2002; Guo et al., 2002). Importantly, the NTE is required for delivery of N-end rule substrates, although it is not needed to bind substrates or ClpA, and shows little evolutionary sequence or length conservation (Hou et al., 2008) (see Figure S1 available online). Crystal structures are known for *E. coli* ClpS bound to the N domain of *E. coli* ClpA, and for *E. coli* or *Caulobacter crescentus* ClpS bound to peptides beginning with Tyr, Phe, Trp, and Leu (Zeth et al., 2002; Guo et al., 2002; Xia et al., 2004; Wang et al., 2008a; Román-Hernández et al., 2009; Schuenemann et al., 2009). In each N-end rule complex, the side chain of the N-end residue is completely buried in a deep hydrophobic pocket, and the α-amino group and first peptide bond make additional contacts with ClpS. Differences in *E. coli* and *C. crescentus* ClpS binding to N-end rule peptides have been proposed (Dougan et al., 2010), but we present evidence here for equivalent recognition by these highly homologous adaptors.

ClpS delivery of substrates to ClpAP must overcome several obstacles. For example, ClpS docks with the highly mobile N domain of ClpA, which could easily leave the substrate more than 80 Å from the axial pore of the D1 AAA+ ring, where unfolding/translocation initiates (Cranz-Mileva et al., 2008; Effantin et al., 2010). A similar issue occurs for the proteasome, where many substrates dock with receptors at sites far from the enzyme's processing center (Striebel et al., 2009). Moreover, some experiments suggest that ClpS and ClpA both recognize the N terminus of N-end rule substrates (Wang et al., 2007). Because the N-terminal side chain is buried in ClpS, substrate handoff to the ClpA pore would need to be actively promoted. However, little is known about the factors that control interactions between N-end rule substrates, ClpS, and ClpA during substrate delivery.

Here, we dissect molecular interactions responsible for assembly of functional delivery complexes. We present evidence for complexes of $ClpA_6$, ClpS, and substrate that differ markedly in stability and delivery activity. The most stable complex requires interactions mediated by the ClpS NTE, a ClpS residue that contacts the substrate N terminus, the substrate N-end

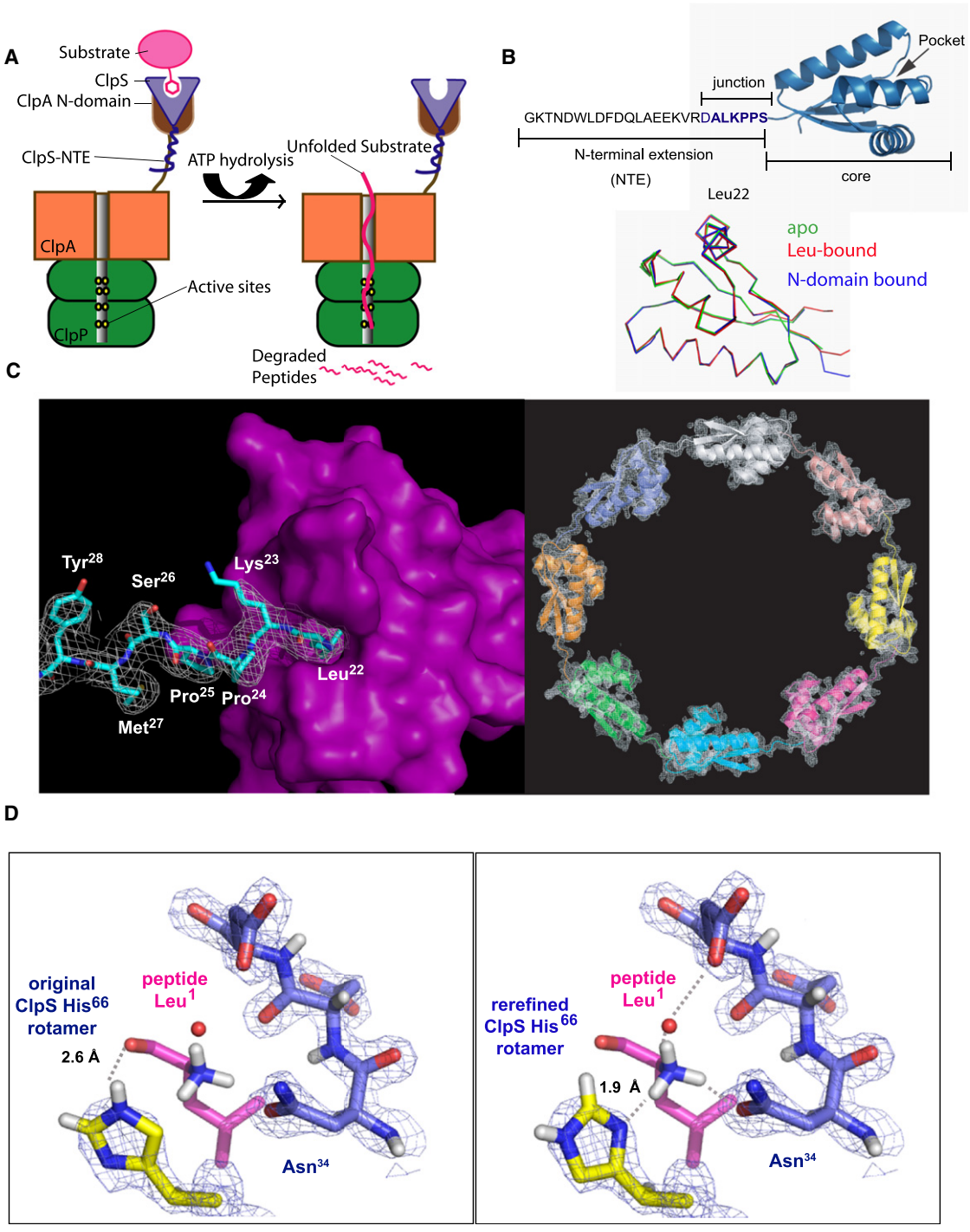

Figure 1. N-End Rule Substrate Recognition

(A) In bacteria, the ClpS adaptor (light blue) recognizes and binds N-end rule substrates (pink) and delivers them for degradation by the ClpAP protease.

(B) (Top) ClpS has a flexible NTE required for N-end rule substrate delivery and a folded $ClpS^{core}$ domain, which binds N-end rule substrates. The ALKPPS sequence at the NTE-core junction is important for adaptor function. (Bottom) Backbone Cα superposition (rmsd < 0.5 Å) of $ClpS^{core}$ (3O1F, green), a peptide-bound ClpS structure (2W9R, red), and ClpS from a complex with the ClpA N domain (1R6O, blue).

(C) (Left panel) In the rerefined 2WA9 structure, the side chain of Leu^{22} from an adjacent ClpS subunit was bound in the N-end rule binding pocket, and density (1σ) for Leu^{22}, Lys^{23}, Pro^{24}, and Pro^{25} was continuous with that for Ser^{26}, Met^{27}, Tyr^{28}, and Lys^{29}, which are part of $ClpS^{core}$. (Right panel) The rerefined map for the 2WA9 structure contained density (1.5 σ) for eight ClpS subunits in the asymmetric unit, arranged head to tail in a ring. The original 2WA9 structure (Schuenemann et al., 2009) had seven ClpS subunits, each with a bound N-end rule peptide.

residue and peptide bond, the AAA+ rings of ClpA, and a sufficiently long linker between the N and D1 domains of ClpA. Efficient substrate delivery also requires NTE residues, which appear to be engaged by the $ClpA_6$ translocation machinery. Our results support a model in which formation of a high-affinity delivery complex (HADC) reduces the mobility of the adaptor-bound substrate complex and positions the substrate's N terminus close to the pore of the D1 AAA+ ring. This staged delivery mechanism illustrates an attractive general model to explain how substrates/adaptors that initially dock far from a AAA+ protease's active center may be localized to the site where they are eventually processed.

RESULTS

ClpS Structures with N-End Rule Peptides Are Highly Conserved and Unstrained

E. coli ClpS has been extensively used for studies of function (Dougan et al., 2002; Erbse et al., 2006; Wang et al., 2007; 2008b; Hou et al., 2008; Román-Hernández et al., 2009; Schuenemann et al., 2009). However, a structure of the free protein had not been solved, leaving open the possibility that a conformational change occurs upon substrate and ClpA N-domain binding. Moreover, conflicting structures suggested that the details of N-end rule recognition might differ in potentially important ways between the *E. coli* and *C. crescentus* adaptors (Dougan et al., 2010). We crystallized *E. coli* $ClpS^{core}$ (residues 26–106) and solved the structure at 1.4 Å resolution (Table 1). The backbone structure was similar to previously reported *E. coli* ClpS structures bound to the ClpA N domain or to N-end rule peptides (Figure 1B; Zeth et al., 2002; Guo et al., 2002; Xia et al., 2004; Schuenemann et al., 2009). Thus, major changes in the conformation of the ClpS core domain do not accompany N-domain or N-end rule substrate binding.

Validation of our $ClpS^{core}$ structure by MolProbity (Davis et al., 2007) revealed excellent geometry (Table 1). By contrast, analysis of the 2W9R, 2WA8, and 2WA9 complexes of *E. coli* ClpS with N-end rule peptides (Schuenemann et al., 2009) revealed bad rotamers, poor bond angles, Ramachandran outliers, Cβ deviations, and unexpected *cis* peptide bonds (Table 1), which could arise if N-end peptide binding introduced strain or if these structures were incorrect. To resolve these issues and gain deeper insight into substrate recognition by ClpS, we rerefined these complexes, producing structures with no geometric anomalies and substantially improved refinement statistics (Table 1). Thus, binding of N-end rule substrates does not introduce strain within ClpS.

Rerefinement allowed us to identify and correct additional errors. For example, the 2WA9 structure purportedly contained a peptide with an N-terminal Trp side chain, which was interpreted to be poorly ordered although it should have been snugly bound in the ClpS hydrophobic pocket (Schuenemann et al., 2009). By contrast, in our rerefined structure, a well-ordered Leu^{22} side chain from the NTE of a neighboring molecule occupied this pocket, with unambiguous electron density connecting the intervening residues to the adjacent $ClpS^{core}$ domain (Figure 1C). This same head-to-tail interaction was observed in eight ClpS molecules, which formed a closed ring in the asymmetric unit (Figure 1C). The original 2WA9 structure contained seven subunits in the asymmetric unit, and the NTE density was incorrectly interpreted as an N-end Trp peptide included during crystallization.

In the apo structure, the His^{66} side chain occupied part of the N-end binding pocket. In the rerefined complexes, the His^{66} ND1 nitrogen hydrogen bonded to the α-amino group of the N-end residue, which required a 180° side-chain flip from the original structures, but the new position fit the electron density well and made better chemical sense (Figure 1D, Figure S2). In the rerefined 2WR9 structure, for example, the unprotonated ND1 nitrogen of His^{66} accepts a hydrogen bond (1.9 Å; 170°) from a peptide -NH_3 proton, whereas the proton on the His^{66} NE2 nitrogen donates a hydrogen bond (2.2 Å; 166°) to a side-chain oxygen from Glu^{94} in a neighboring molecule (Figure S2). By contrast, when we added hydrogens to the original 2WR9 structure using REDUCE (Word et al., 1999), the nonpolar HD2 hydrogen of the His^{66} ring clashed with a peptide NH_3 proton, a hydrogen bond between the peptide carbonyl oxygen and the proton on the NE2 nitrogen had poor geometry (2.6 Å; 117°), and the close interaction with the Glu^{94} carboxylate involved a nonpolar hydrogen on the His^{66} ring. Importantly, in the rerefined complexes, contacts between *E. coli* ClpS and the N-terminal substrate residue were essentially indistinguishable from those observed in complexes of N-end rule peptides with *C. crescentus* ClpS, including hydrogen bonds with the side chains of Asn^{34} (Figure 1D) and a water molecule that bridges the α-amino group and Asp^{35} side chain (Wang et al., 2008a; Román-Hernández et al., 2009). We conclude that the mechanism of recognition of N-end rule peptides by ClpS is highly conserved.

Enhanced N-End Rule Affinity Requires the ClpS NTE and $ClpA_6$

The NTE is required for substrate delivery (Hou et al., 2008), but its functional role is obscure. We established that the NTE does not affect binary binding to N-end rule substrates, as intact ClpS and $ClpS^{core}$ bound to a fluorescent N-end rule peptide (LLYVQRDSKEC-fl) with comparable affinities (~3 μM) in assays monitored by fluorescence anisotropy (Figure 2A). Strikingly, ClpS binding to this peptide was much tighter (~40 nM) in the presence of ClpA and ATPγS, which stabilizes ClpA hexamers (Figure 2B). The final anisotropy value was also higher with ClpA present, as expected for slower tumbling of the larger ClpA-ClpS-peptide complex compared to a ClpS-peptide complex. Importantly, tighter binding was not observed when

(D) In the rerefined 2W9R structure (right panel), the correct rotamer of the His^{66} side chain makes hydrogen bonds (dashed lines) with the α-NH_3 group of the bound N-end peptide and fits nicely into the electron density. In the original 2W9R structure (Schuenemann et al., 2009; left panel), His^{66} rotamer chosen makes a poor hydrogen bond with the carbonyl oxygen of the first peptide residue and does not fit optimally into the electron density. In both panels, the electron density (1.25σ) is from our rerefined map.

Table 1. Refinement Statistics

PDB code	3O1F	2W9R	3O2H	2WA8	3O2B	2WA9	3O2O
E. coli ClpS residues	26–106	2–108[b]	2–106	2–106		2–108[b]	2–106[c]
N-end peptide	none	LVKSKATNLLY		FRSKGEELFT		unclear[d]	none
Space group	P1	P1		$P12_11$		C2	
Unit cell a =	28.0 Å	28.1 Å		32.2 Å		171.9 Å	
Unit cell b =	28.1 Å	28.2 Å		58.4 Å		155.9 Å	
Unit cell c =	51.6 Å	38.9 Å		56.4 Å		71.2 Å	
Unit cell α =	80.5°	97.4°		90.0°		90.0°	
Unit cell β =	77.9°	106.5°		101.9°		114.6°	
Unit cell γ =	72.3°	92.4°		90.0°		90.0°	
Subunits/peptides per asu	2/0	1/1		2/2		7/7	8/0
Refinement resolution	22.5–1.4 Å	25.0–1.7 Å		30.2–2.15 Å	30.2–2.05 Å	25.0–2.9 Å	
Wavelength	1.54 Å	0.978 Å		1.071 Å		1.071 Å	
R_{sym} (%)	3.6	3.9 (20.9)		11.3 (45.1)		13.7 (73.6)	
Unique reflections	23,635	11,540		9,909	12,292	19,203	
Completeness (%)	82.4 (32)	91.1 (86.1)		94.0 (90.5)	94.9 (96.0)	99.3 (96.3)	
Data redundancy	3.7 (3.1)	2.2 (2.0)		2.9 (2.7)		7.5 (7.3)	
Average I/σI	25.1 (5.2)	12.4 (3.9)		6.5 (2.3)		11 (2.0)	
R_{work} (%)	17.3 (21.7)	22.6 (27.8)	19.7 (25.6)	22.5 (26.0)	21.1 (27.1)	23.7 (26.1)	17.3 (29.4)
R_{free} (%)	19.7 (21.0)	25.4 (32.8)	22.7 (33.2)	26.8 (33.5)	24.8 (31.8)	24.8 (28.5)	20.1 (32.1)
TLS	no	yes[e]	no	no	no	yes	no
Rmsd bond lengths (Å)	0.007	0.009	0.009	0.010	0.006	0.015	0.005
Rmsd bond angles (°)	1.19	1.19	1.17	1.54	1.02	1.57	0.79
Total protein atoms including H	2637	861 (no H)	1712	1660 (no H)	3199	4880 (no H)	10767
Solvent atoms	402	68	128	91	140	0	0
Average B value	17.9	22.1	24.1	33.2	33.6	50.0	73.7
Ramachandran[a]							
Favored/allowed/disallowed (%)	100/0/0	100/0/0	100/0/0	93.5/3.0/3.5	100/0/0	94.4/2.0/3.6	99.5/0.5/0
Favorable rotamers (%)[a]	100	93.6	100	89.9	100	89.7	100
Clash score[a]	0.0	5.8	0.0	18.7	0	17.1	0
Cβ deviations > 0.25 Å[a]	0	0	0	3	0	4	0
Residues with bad angles[a]	0	0	0	1	0		0
Cis peptide bonds	0	0	0	8	0	0	0

Numbers in parentheses represent values for the highest-resolution bin. Unit cell and data collection statistics for the rerefined structures are from Schuenemann et al. (2009). $R_{sym} = S_h S_j |I_j(h) - < I(h) > | / S_h S_j < I(h) >$, where $I_j(h)$ is the j^{th} reflection of index h and $< I(h) >$ is the average intensity of all observations of I(h). $R_{work} = S_h |F_{obs}(h) - F_{calc}(h)| / S_h |F_{obs}(h)|$, calculated over the 93%–95% of the data in the working set. R_{free} equivalent to R_{work} except calculated over 5%–7% of the data assigned to the test set.

[a] Favorable/allowed/disallowed Ramachandran angles, favorable rotamers, Cβ deviations, residues with bad angles, and the clash score (number of steric overlaps $\geq$ 0.4 Å per 1000 atoms) were calculated using MolProbity (Davis et al., 2007).

[b] The original 2W9R and 2WA9 structures (Schuenemann et al., 2009) contain two additional C-terminal residues that are not present in the protein sequence. In our rerefined structures, there was no density for these "extra" residues, and the chain terminated with Ala^{106} as expected.

[c] As discussed in the text, it is possible that the polypeptide was cleaved between Ala^{21} and Leu^{22}.

[d] The peptide sequence is listed as LLT in the pdb file but as WRSKGEELFTGV in Schuenemann et al. (2009). In our rerefined structure, there was no peptide. Instead, an N-terminal segment of a neighboring ClpS molecule occupied the binding pocket.

[e] ANISOU records are included in the 2W9R PDB file, although the header reports no TLS groups.

$ClpS^{core}$ was used in place of intact ClpS, when the N domain of ClpA or $^{\Delta N}$ClpA were used in place of ClpA, or when ATPγS was omitted (Figures 2A and 2B; data not shown). Thus, N-end rule binding by ClpS is substantially strengthened in an NTE-dependent manner by interactions with the N domain and hexameric ring of $ClpA_6$.

ClpS Binds $ClpA_6$ More Tightly in the Presence of N-End Rule Peptides

We constructed ClpS* (C73V; C101S; E96C), which contains one surface-exposed cysteine and was fully active in multiple functional assays (data not shown), labeled it with fluorescein ($ClpS^{*F}$), and measured fluorescence anisotropy in the presence

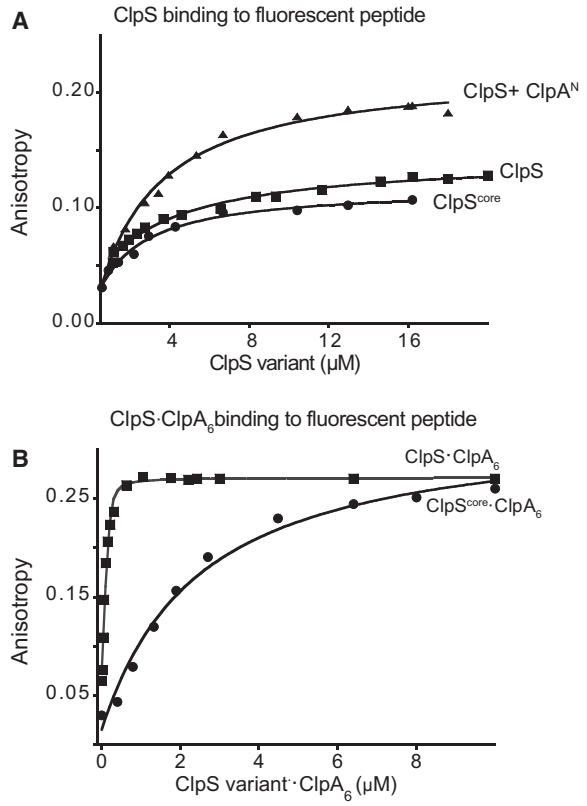

Figure 2. N-End Rule Degrons Bind More Tightly to the ClpS-ClpA$_6$ Complex

(A) A fluorescent N-end rule peptide (LLYVQRDSKEC-fl; 200 nM) was bound with similar affinities (K_D ~3 μM) by ClpS, by ClpS^{core}, and by ClpS in complex with the ClpA N domain, as assayed by changes in anisotropy. The molecular weights and maximum anisotropies of each complex differ.

(B) Increasing concentrations of 1:1 molar mixtures of ClpA$_6$ and ClpS or ClpS^{core} were titrated against the LLYVQRDSKEC-fl peptide (100 nM). The ClpS-ClpA$_6$ complex bound more tightly (K_{app} = 42 ± 6 nM) than the ClpS^{core}-ClpA$_6$ complex (K_{app} = 1.5 ± 0.25 μM), demonstrating that the ClpS NTE is required for affinity enhancement. Assays contained 4 mM ATPγS to promote ClpA hexamer formation. Reported K_{app} values are averages (n ≥ 2) with errors calculated as SQRT(K-K_{avg})^2/n).

of increasing concentrations of ClpA$_6$ (stabilized by ATPγS). The fitted K_{app} value was ~180 nM (Figure 3A). Next, we assayed binding in the presence of excess LLYVQRDSKEC, a Phe-Val dipeptide, or Trp-CONH$_2$, all of which have good N-end rule side chains. In each case, ClpA$_6$ bound ClpS^{*F} at least 9-fold more tightly than observed with a MLYVQRDSKEC peptide or in the absence of ligand (Figure 3A). Although binding was too tight to calculate accurate K_{app} values, Trp-CONH$_2$ enhanced ClpA$_6$ affinity for ClpS^{*F} as well as the longer N-end rule peptides, indicating that the N-terminal residue and a few nearby atoms play the dominant role in enhanced binding.

If there are no ligand-induced conformational changes in ClpS, as the structures argue, then how does Trp-CONH$_2$ enhance ClpA$_6$ binding to ClpS? Because the side chain of Trp-CONH$_2$ would be buried in ClpS, binding stimulation might involve contacts between ClpA$_6$ and exposed main-chain atoms of Trp-CONH$_2$, or contacts between ClpA$_6$ and ClpS side chains whose conformations are stabilized by contacts with Trp-CONH$_2$. Therefore, we tested if His^{66} in ClpS might participate in binding enhancement, as this residue contacts the substrate N terminus (Figure 1D), the H66A mutation increased K_M and reduced V_{max} for ClpAP degradation of N-end rule substrates (Wang et al., 2008a), and His^{66} adopted different conformations in the apo and peptide-bound structures of *E. coli* ClpS (Figure 3B). Importantly, we found that peptide-free ^{H66A}ClpS^{*F} bound ClpA$_6$ nearly as well as ClpS^{*F}, but peptide-bound ^{H66A}ClpS^{*F} bound ClpA$_6$ ~9-fold more weakly than the parent (Figure 3C). Thus, this mutant does not form the high-affinity complex. Although the H66A mutation reduces N-end substrate affinity (Figure 3D), the experiment in Figure 3C was performed using a peptide concentration 35-fold higher than K_{app} for ^{H66A}ClpS•ClpA$_6$ binding, ensuring that most mutant ClpS molecules were peptide bound. We conclude that the His^{66} side chain stabilizes a high-affinity complex of ClpA$_6$, ClpS, and substrate.

De Donatis et al. (2010) reported that NTE deletion reduced binary ClpA$_6$ affinity. We found that NTE deletion in a ClpS^{*F} variant reduced binary ClpA$_6$ affinity ~10-fold and also reduced the anisotropy observed at binding saturation (Figure S3). These results show that the NTE helps stabilize the ClpS•ClpA$_6$ complex, both in the presence and absence of substrate, and suggest that the NTE-mediated interaction reduces the segmental mobility of ClpA$_6$-bound ClpS.

ClpS-ClpA$_6$ Collaboration Requires Mobility of the ClpA N Domain

ClpS^{core} docks with the ClpA N domain, which is linked to the D1 ring by a 26-residue tether. Using a ClpA variant with a four-residue tether ($^{\Delta L}$ClpA; Cranz-Mileva et al., 2008) allowed us to probe the importance of linker length. In the absence of substrate, ClpS^{*F} bound ClpA$_6$ and $^{\Delta L}$ClpA$_6$ equally well (Figure 3E), suggesting that the shorter linker does not prevent formation of the NTE-mediated contacts with ClpA$_6$. Importantly, however, when binding was measured in the presence of N-end rule peptide, $^{\Delta L}$ClpA$_6$ showed much weaker binding (Figure 3E). Thus, an N-D1 linker of sufficient length is important in forming stable ternary complexes with ClpS and N-end rule substrates. Analysis of the steady-state kinetics of ClpAPS degradation of YLFVQELA-GFP revealed a 7-fold weaker K_M and 3-fold lower V_{max} when $^{\Delta L}$ClpA$_6$ was substituted for wild-type ClpA$_6$ (Figure 3F). Thus, the longer linker is also required for efficient substrate delivery to ClpAP. Using a different substrate, Cranz-Mileva et al. (2008) also found defects in degradation using $^{\Delta L}$ClpA$_6$, albeit significantly smaller than those shown in Figure 3F.

Defining NTE Lengths Required for Efficient ClpS Delivery and Formation of High-Affinity Complexes

To probe the importance of NTE length, we purified ClpS mutants with N-terminal truncations from 3 to 20 amino acids and assayed their ability to slow ATP hydrolysis by ClpA and to deliver YLFVQELA-GFP for ClpAP degradation (Figure 4A). Strikingly, a precipitous decline in delivery and loss of ability to suppress ATPase rates occurred over a very narrow truncation range defined by the Met-Leu^{13} and Met-Ala^{14} variants. To investigate this delivery defect in greater detail, we determined

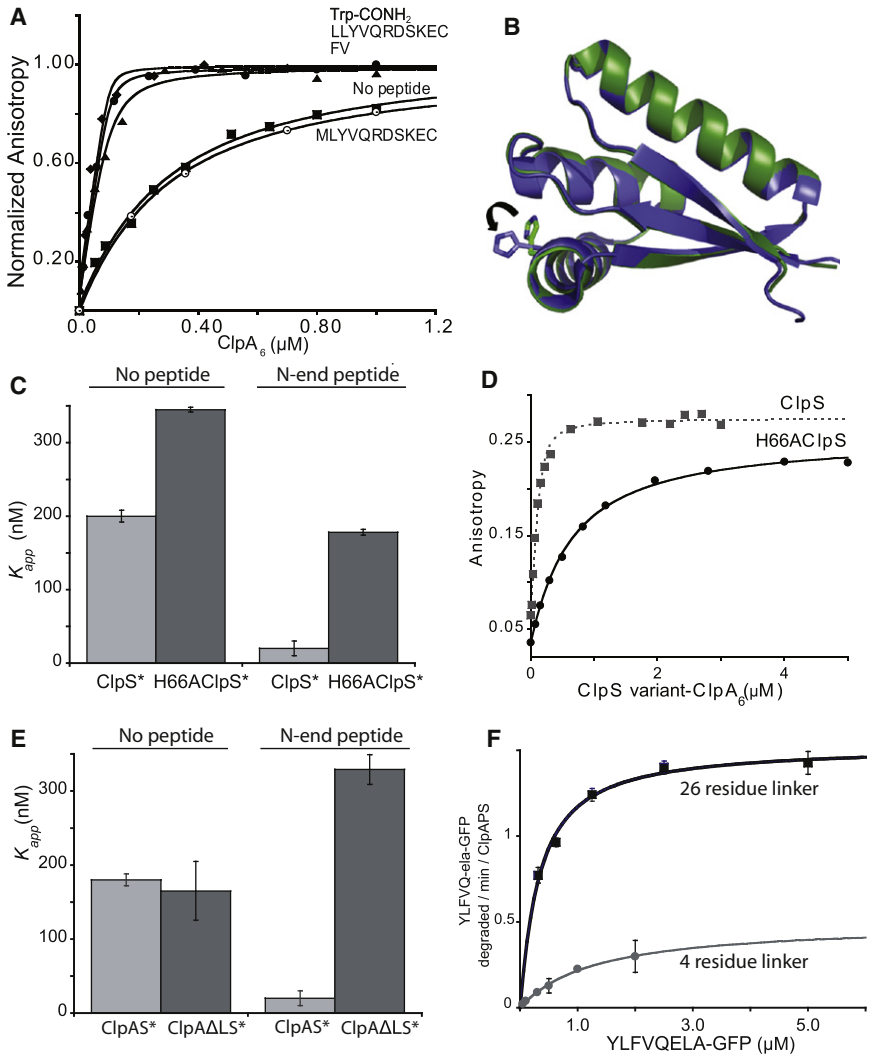

Figure 3. ClpS Binds $ClpA_6$ More Tightly in the Presence of N-End Rule Peptides

(A) As assayed by anisotropy, $ClpA_6$ bound 200 nM fluorescent $ClpS^{*F}$ tightly in the presence of 20 μM Trp-$CONH_2$, LLYVQRDSKEC, or FV N-end rule peptides (K_{app} < 20 nM) and more weakly in the absence of peptide or with 20 μM MLYVQRD SKEC peptide (K_{app} ~180 nM).

(B) The H66 residue of ClpS is one of the side chains involved in the formation of one of the three hydrogen bonds that the adaptor forms with the α-amino group of the N-end degron. Overlay of the apo (green, PDB 3O1F) and the peptide-bound (blue, 2W9R) crystal structures of ClpS reveals no major global changes occur upon peptide binding. The most substantial change is the rotation of the H66 side chain, which appears to need to move away from the pocket in the apo form to accommodate the N-degron in the peptide binding site.

(C) $ClpA_6$-bound $ClpS^{*F}$ (K_D = 200 ± 6 nM) and $^{H66A}ClpS^{*F}$ (K_D = 345 ± 3 nM) with similar affinities. Addition of 20 μM LLYVQRDSKEC N-end rule peptide enhanced $ClpA_6$ affinity for $ClpS^{*F}$ substantially (K_{app} = 20 ± 10 nM) but increased affinity for $^{H66A}ClpS^{*F}$ only modestly (K_{app} = 178 ± 4 nM).

(D) $^{H66A}ClpS$-$ClpA_6$ complex binds more weakly to an N-end rule fluorescent peptide (LLYVQRD-SKEC-fl) when compared to ClpS-$ClpA_6$ (K_{app} = 560 nM versus K_{app} = 42 ± 6 nM for wild-type).

(E) An N-end rule peptide (LLYVQRDSKEC; 20 μM) enhanced binding of $ClpS^{*F}$ to $ClpA_6$ but not to $^{\Delta L}ClpA_6$, which has shorter linker between the N and D1 domains (Cranz-Mileva et al., 2008).

(F) Michaelis-Menten plots showed that substituting $^{\Delta L}ClpA_6$ (four-residue linker) for $ClpA_6$ (26-residue linker) decreased K_M and V_{max} for ClpAPS degradation (100 nM $ClpA_6$ or $^{\Delta L}ClpA_6$; 200 nm $ClpP_{14}$; 600 nm ClpS) of the N-end rule substrate YLFVQELA-GFP. Reported K_D, K_M, and K_{app} values are averages (n ≥ 2) with errors calculated as SQRT(K-K_{avg})^2/n).

the steady-state kinetics of ClpAP degradation of different concentrations of YLFVQELA-GFP in the presence of ClpS or the variants starting with Met-Leu[13] and Met-Ala[14] (Figure 4B). The Met-Leu[13] mutant delivered the substrate with a 1.3-fold reduction in V_{max} compared to ClpS. By contrast, delivery by the Met--Ala[14] variant displayed a 7.5-fold decrease in V_{max}. These results demonstrate that the ClpS NTE must have a critical minimum length to promote efficient delivery to ClpAP.

We also determined K_{app} values for binding of several ClpS-NTE variants to a fluorescent N-end rule peptide in the presence of $ClpA_6$/ATPγS (Figure 4C). Mutants beginning at Asp^{20} or earlier formed relatively stable substrate complexes with $ClpA_6$ (K_{app} 80–120 nM), albeit less stable than the wild-type ClpS complex. Thus, an NTE extending past residue 14 is not required for relatively stable ternary-complex formation but is needed for efficient substrate delivery. Affinity was weakened further when the truncated ClpS variant began with Leu^{22} (~300 nM) and substantially more when it started at Ser^{26} ($ClpS^{core}$; ~1500 nM; Figure 2C; Figure 4C). These results establish that four to five residues at the junction between the NTE and $ClpS^{core}$ are important for stabilizing high-affinity complexes. This junction sequence was substantially conserved among orthologs, whereas the rest of the NTE showed almost no sequence conservation (Figure S1; Zeth et al., 2002; Guo et al., 2002), supporting a model in which the NTE-junction residues form specific docking contacts with ClpA.

FeBABE Mapping Places the ClpS NTE Near the ClpA Pore

To probe regions of contact between the NTE and ClpA, we attached FeBABE to residue 12 of $^{Q12C}ClpS$ (Figure 5A). In the presence of ascorbic acid and hydrogen peroxide, the Fe^{3+} atom in the NTE-bound FeBABE generates free radicals which can cleave regions of ClpA in close proximity. ClpS was mixed with ClpA containing a C-terminal FLAG tag in the presence of ATPγS, ADP, or no nucleotide. After 30 min, cleavage was initiated, allowed to proceed for 30 s, quenched, and the products analyzed by SDS-PAGE. In presence of ATPγS, FeBABE

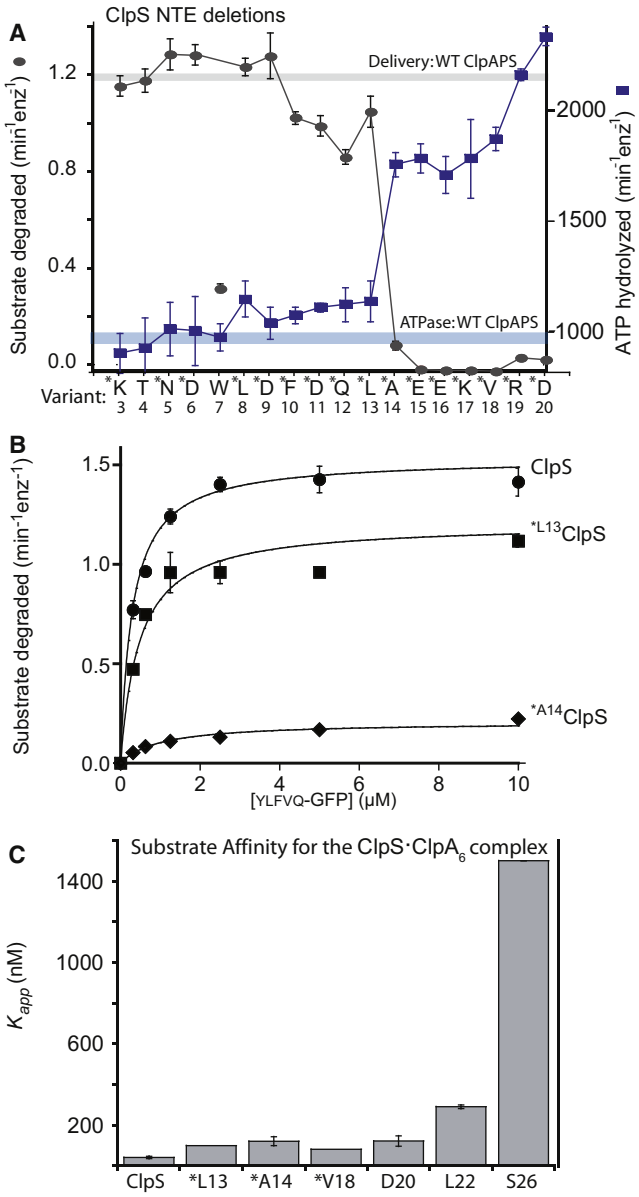

Figure 4. A Minimal NTE Length Is Required for ClpS Function

(A) ClpS variants (1 μM) with N-terminal truncations were assayed for delivery of YLFVQELA-GFP (1 μM) for ClpAP degradation (gray curve) and for effects on ClpAP ATP hydrolysis (blue curve) using 100 nM $ClpA_6$ and 270 nM $ClpP_{14}$ for both assays. Data points represent averages (n = 3) ± 1 SD. Each ClpS variant is named by the first wild-type residue in the construct. Those marked with an asterisk contain an additional N-terminal methionine and are therefore one residue longer than the labels indicate; these mutants were expressed as SUMO-fusion proteins and cleaved in vitro (see the Experimental Procedures) or were expressed as standard nonfusion proteins but retained the initiator Met (verified by mass spectrometry). The T4 and W7 variants were also expressed as standard nonfusion proteins, but mass spectrometry and/or N-terminal sequencing showed that the initiator Met was removed from both of these proteins. Note the sharp activity transitions between *L13 ClpS (starting $Met^{12}Leu^{13}$) and *A14 ClpS (starting $Met^{13}Ala^{14}$). The processing of the W7 variant is inconsistent with canonical methionine aminopeptidase activity and generates a good N-end rule residue, which may be responsible for the poor activity of this ClpS variant in delivering other N-end rule substrates.

(B) Michaelis-Menten plots of YLFVQELA-GFP degradation by ClpAP and ClpS or variants (100 nM $ClpA_6$; 200 nm $ClpP_{14}$; 600 nm ClpS or variants). Wild-type ClpS and *L13 ClpS (beginning $Met^{12}Leu^{13}Ala^{14}$) supported roughly similar steady-state degradation kinetics, but delivery by *A14 ClpS (beginning $Met^{13}Ala^{14}Glu^{15}$) resulted in a substantial decrease in V_{max}. Thus, the NTE must have a critical minimal length to support efficient substrate delivery. The solid lines are a global fit to a model in which the ClpS-substrate complex binds ClpA in an initial bimolecular step (K_1 = 1.1 μM) and then is engaged for degradation in a second unimolecular step (K_2), which depends on NTE length. In this model, apparent $V_{max} = E_{total} \bullet k_{deg}/(1 + K_2)$ and apparent $K_M = K_1 \bullet K_2/(1 + K_2)$. For the fits shown, the k_{deg} value was 2.1 min^{-1} and the K_2 values were 0.37 (wild-type ClpS), 0.74 (*L13 ClpS), and 9.2 (*A14 ClpS).

(C) Binding to an N-end rule peptide (LLYVQRDSKEC-fl; 150 nM) by complexes of $ClpA_6$ with ClpS variants (1 ClpS per $ClpA_6$) showed that ClpS junction residues are important for formation of the HADC. Variants marked * have an additional N-terminal methionine. Apparent affinity constants were 43 nM (wild-type ClpS), 100 nM (*L13), 130 nM (*A14), 83 nM (*V18), 130 nM (D20), 290 nM (L22), and 1500 nM (S26).

cleavage resulted in two fragments of ~50 kDa and two of ~29 kDa either in the absence (Figure 5A) or presence (data not shown) of N-end rule peptides. No specific cleavage products were observed without nucleotide or with ADP, suggesting that cleavage requires ATPγS-dependent formation of $ClpA_6$•ClpS complexes (Figure 5A).

Western blots using anti-FLAG antibody indicated that the larger FeBABE cleavage products corresponded to the C-terminal portion of ClpA and the smaller bands were N-terminal segments (data not shown). Edman sequencing of these products was unsuccessful. However, based on molecular-weight standards and fragments produced by cleavage before cysteines in the Y259C, K265C, and K268C variants of ClpA, FeBABE cleavage appeared to occur near ClpA residue 260 (Figure S4). Residues 259–268 are located near the axial pore of the D1 AAA+ ring of ClpA. The FeBABE-ClpS linkage would allow the reagent to reach regions of ClpA within ~12 Å of the site of NTE attachment. Mapping these potential contacts on a model of the ClpA hexamer suggested that the ClpS NTE could physically contact the central pore of $ClpA_6$ and/or the top of the D1 ring (Figure 5B).

The NTE Is a Degradation Signal, but ClpS Resists ClpAP Proteolysis

ClpAP does not degrade ClpS (Dougan et al., 2002). Nevertheless, because the NTE makes contacts near the ClpA pore, we hypothesized that it might be engaged by the translocation/unfolding machinery. To test this model, we appended the mature NTE of *E. coli* ClpS (residues 2–26) to the N terminus of GFP and assayed degradation. Untagged GFP is not degraded by ClpAP (Weber-Ban et al., 1999), but the NTE-fusion protein was efficiently degraded (Figure 5C), with a K_M of 16 μM and V_{max} similar to other GFP substrates. These results support a model in which the ClpA pore can engage the ClpS NTE, but the ClpS core domain resists proteolysis. To confirm that $ClpS^{core}$ is refractory to degradation, we purified H_6-SUMO-NTE-$ClpS^{core}$, H_6-SUMO-$ClpS^{core}$, and YLFVQELA-GFP-NTE-$ClpS^{core}$ fusion proteins and assayed ClpAP proteolysis. In each case, partial proteolysis was observed (Figures 5D and 5E), but Edman degradation of the resistant fragment demonstrated

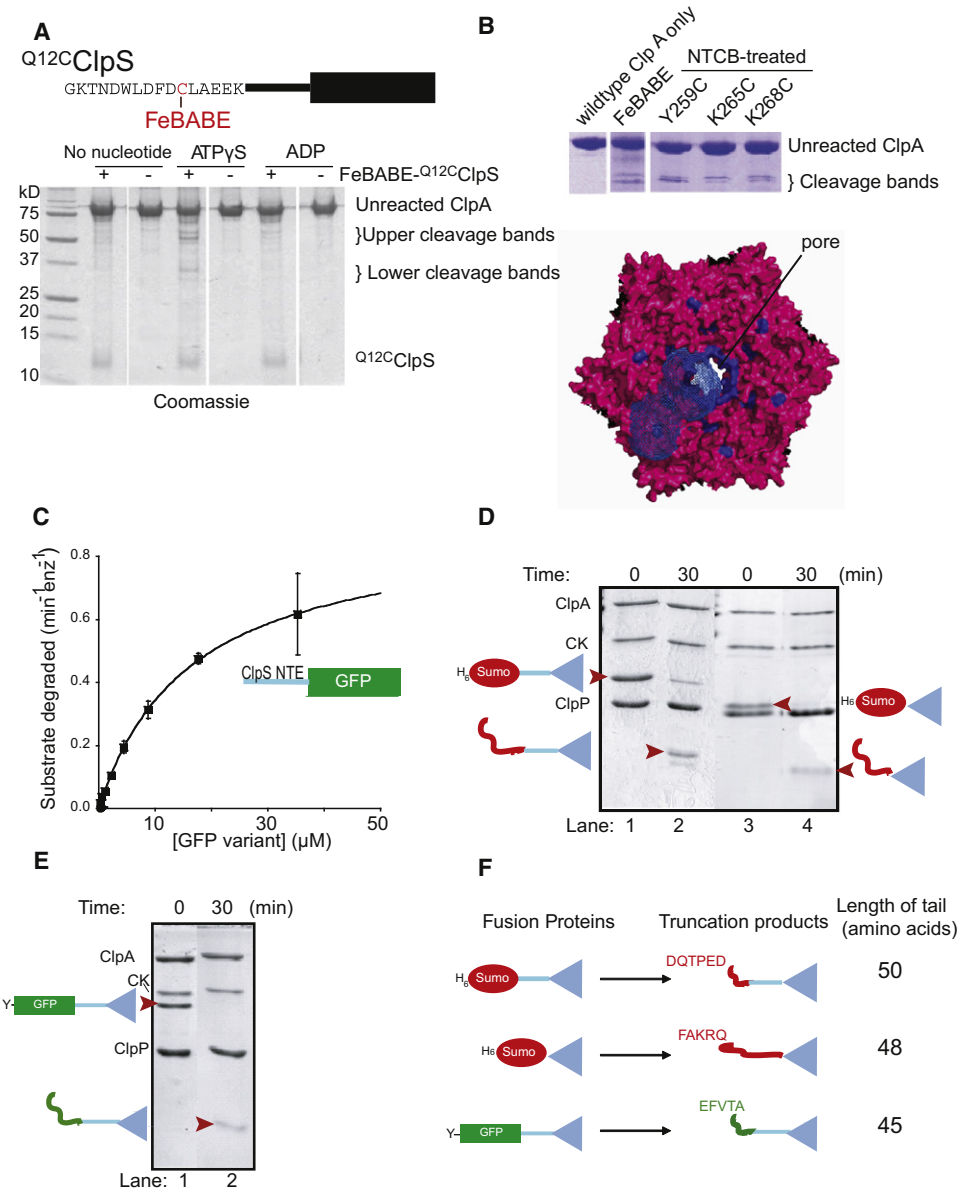

Figure 5. The ClpS NTE Contacts ClpA Near the Axial Pore

(A) (Top) FeBABE was attached to residue 12 of ^{Q12C}ClpS variant for cleavage studies. (Bottom) As assayed by SDS-PAGE, cleavage of ClpA required FeBABE-modified ^{Q12C}ClpS and ATPγS.

(B) ClpA residues 259–268 are highlighted in blue in a top view of a model of the hexameric D1 ring (Guo et al., 2002). In one ClpA subunit, blue wire shading shows regions within 12 Å of residues 259–268, which represents the approximate reach of the tethered FeBABE.

(C) A substrate consisting of residues 2–26 of ClpS fused to GFP was efficiently degraded by ClpAP, as shown by Michaelis-Menten analysis (K_M = 16.4 μM; V_{max} = 0.62 min^{-1} enz^{-1}).

(D) Assays monitored by SDS-PAGE showed that ClpAP only partially degraded the H_6-Sumo-ClpS and H_6-Sumo-ClpS^{core} fusion proteins, resulting in truncated products of a lower molecular weight (marked by red arrowheads in lanes 2 and 4).

(E) ClpAP partially degraded the YLFVQELA-GFP-ClpS fusion protein, resulting in a lower molecular weight truncation product (marked by a red arrowhead in lane 2).

(F) Depiction of the ClpS fusion proteins used to test degradation by ClpAP (left) and the corresponding truncation products produced by degradation (right). N-terminal sequencing of the truncation products revealed that the new N termini corresponded to an internal sequence in the protein fused to ClpS (either Sumo or GFP). The truncation products consisted of the ClpS core and an additional N-terminal tail of 45–50 amino acids.

that ClpS^{core} remained intact, as did an N-terminal tail of 45–50 amino acids before the core domain (Figure 5F). Tails of this length result when AAA+ proteases are unable to unfold a very stable domain in the midst of a multidomain substrate (Lee et al., 2001; Koodathingal et al., 2009), strongly supporting a model in which ClpAP cannot unfold or degrade the ClpS^{core}

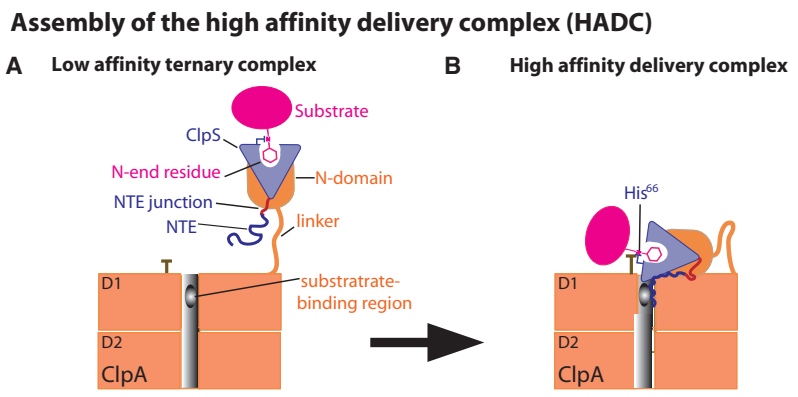

Figure 6. Model for Staged Delivery of N-End Rule Substrates

(A) Independent binding of ClpS to the ClpA N domain and of the substrate N-end residue in the ClpS pocket results in a low-affinity ternary complex.

(B) A HADC is stabilized by additional interactions between the D1 ring of ClpA and NTE-junction residues and between the D1 ring, the His^{66} side chain of ClpS, and the N-end residue of the substrate.

(C) Translocation-mediated ClpA tugging on the NTE distorts the $ClpS^{core}$ structure, weakens ClpS interactions with the N-end residue, and facilitates transfer of the N-degron of the substrate to a site in the ClpA pore.

(D) ClpS slips from the grasp of ClpA, clearing the pore and allowing subsequent degradation of the N-end rule substrate.

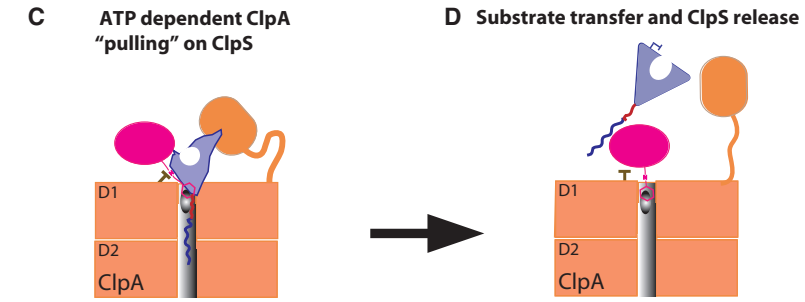

domain. As discussed below, this degradation-resistant character of ClpS is likely to be critical for its function as an efficient adaptor.

DISCUSSION

The work presented here elucidates important new aspects of the molecular mechanism of ClpS delivery and ClpAP degradation of N-end rule substrates. Our current view of these processes is shown in the model of Figure 6, which begins with formation of a low-affinity ternary complex (LATC; Figure 6A), proceeds to a HADC (Figure 6B), and ends with active substrate handoff from ClpS to ClpA (Figures 6C and 6D). As illustrated in Figure 6A, uncoupled sets of binary contacts between ClpS and the N-end rule substrate and between $ClpS^{core}$ and the ClpA N domain stabilize the LATC. Formation of the HADC involves additional interactions mediated by junction residues of the NTE of ClpS, by His^{66} of ClpS, by the N-end residue of the substrate, and by the D1 ring of ClpA (Figure 6B). The ClpS•substrate portion of the complex is highly mobile in the LATC, because of the flexible tethering of the N domain to the D1 ring of ClpA, but is constrained in the HADC by additional contacts with the D1 ring.

The properties of the LATC are based on previous studies of the interaction of ClpS with substrates or the N domain of ClpA. Our current work supports the existence of the HADC and defines many of its properties. For example, we find that degrons containing just the N-end residue and peptide bond enhance ClpS affinity for $ClpA_6$ and are bound far more tightly by ClpS and $ClpA_6$ together than by either individual protein. Moreover, high-affinity binding requires multiple regions of ClpS (including the junction region of the NTE and His^{66}, which contacts the N-end residue of the substrate), as well as the AAA+ body of ClpA and a suitably long linker between the ClpA D1 ring and N domain. Consistent with the Figures 6A and 6B models, we find that the mobility of the ClpS portion of complexes with ClpA is higher when the NTE is absent. Work presented here and previously (Hou et al., 2008; Wang et al., 2008a; Schuenemann et al., 2009) shows that mutation of His^{66} or deletion of the NTE severely compromises ClpS delivery of N-degron substrates to ClpAP, indicating that formation of the HADC is a critical step in substrate delivery.

It is not currently known what parts of the AAA+ body of ClpA make contacts with the junction residues of the NTE or with His^{66} and the N-end residue in the HADC, but our studies set the stage for future experiments to define these interactions in greater molecular detail. FeBABE cleavage experiments do show that residues near the center of the NTE can contact the D1 AAA+ ring of $ClpA_6$, and given the size of ClpS, other contacts with the AAA+ body of $ClpA_6$ would likely also be restricted to the D1 ring. For example, a residue in the D1 ring of ClpA could contact the His^{66} of ClpS and stabilize its interaction with the α-amino group of the N-degron, explaining the importance of all of these elements in stabilizing the HADC. Alternatively, the conformation of the His^{66} side chain could change in the HADC, allowing one set of D1 interactions with His^{66} and another set of interactions with the N-degron. Interestingly, a sufficiently long linker between the ClpA N domain and AAA+ ring is needed to allow formation of the ClpA contacts mediated by the N-end degron and ClpS binding pocket.

In addition to its role in delivery of N-degron substrates, ClpS binding prevents recognition and degradation of other types of substrates by ClpAP (Dougan et al., 2002). In the absence of N-end rule substrates, it would be counterproductive if ClpS bound ClpA too tightly, as this would preclude degradation of

other substrates. However, we find that ClpS binds $ClpA_6$ ~10-fold more tightly when N-degron substrates are present, providing an elegant solution to this problem. Substrate-dependent affinity enhancement would help to ensure the formation of a ClpAPS complex when N-end rule substrates were available but also keep ClpAP largely free to perform other functions when these substrates were absent.

Our working model for substrate delivery culminates with engagement of the substrate N-degron by the ClpA pore (Figure 6). A key feature of this model is binding of a portion of the ClpS NTE in the ClpA pore (Figure 6B), allowing the translocation/unfolding machinery to pull on ClpS and facilitate transfer of the N-degron from ClpS to ClpA (Figures 6C and 6D). Although aspects of the transfer model are speculative, it accounts for many experimental observations. For example, we found that a truncated ClpS variant beginning at NTE-residue 13 mediated efficient substrate degradation, whereas deleting one additional NTE residue dramatically reduced delivery. The presence of the extra residue could allow the NTE to reach a binding site in the $ClpA_6$ pore that was critical for initiating substrate delivery. Indeed, our FeBABE cleavage results suggest that this central region of the NTE could contact the pore of the ClpA D1 ring. Engagement of the NTE by the ClpA pore is also supported by our finding that appending the ClpS NTE to GFP, a protein which is not normally degraded, results in efficient ClpAP degradation. Despite NTE engagement, our results also show that the folded portion of ClpS resists ClpAP degradation. In combination, these results account for our observation that delivery-competent NTE truncations result in lower ClpA ATPase rates than delivery-incompetent truncations. For example, AAA+ unfoldases hydrolyze ATP more slowly during attempts to unfold a protein (Kenniston et al., 2003; Wolfgang and Weber-Ban, 2009), and the lower ATPase rates seen using delivery-competent NTE truncations are therefore consistent with failed ClpA attempts to unfold ClpS.

How could ClpA tugging on ClpS facilitate handoff of N-end rule substrates? Given that the NTE is distant from the ClpS substrate-binding pocket, an attractive model is that translocation-mediated pulling on the NTE deforms $ClpS^{core}$, facilitating transfer of the N-end degron to a site in the ClpA pore (Figure 6C). This model requires independent recognition of the N-degron by ClpA, which is supported by the observation that ClpAP alone can recognize and degrade N-end rule substrates, albeit with relatively low K_Ms compared to values obtained with ClpS (Wang et al., 2007). Moreover, in resisting unfolding, ClpS could slip from the grasp of ClpA, as observed for other difficult-to-unfold proteins (Kenniston et al., 2005), clearing the pore as a prelude to substrate degradation (Figure 6D). Experiments with the related ClpXP enzyme also reveal that multiple polypeptide chains can simultaneously occupy the pore (Burton et al., 2001; Bolon et al., 2004).

There are parallels between the Figure 6 model and the delivery of ssrA-tagged substrates to the ClpXP protease by the SspB adaptor. For example, one region of SspB binds the N domain of ClpX, another part of SspB binds to a segment of the ssrA degron, a different part of this degron binds to the ClpX pore, and each binary interaction is substantially weaker than the overall ternary interaction (Levchenko et al., 2000, 2003; Wah et al., 2003; Bolon et al., 2004; Martin et al., 2008). Because the ssrA tag of the substrate is positioned in the pore of the ClpX AAA+ ring in the high-affinity complex, ATP-fueled translocation allows tag contacts with the adaptor to be broken at the same time that degradation is initiated.

Assembly of increasingly stable macromolecular complexes frequently drives biological recognition. This mechanism provides directionality by proceeding downhill to a thermodynamic minimum but also results in an energy well from which spontaneous escape is difficult, creating a problem if the high-affinity complex is not the final product. For example, recombination catalyzed by MuA transposase is driven by increasingly stable protein-DNA complexes, which eventually must be disassembled in an ATP-dependent process by ClpX (Burton and Baker, 2005). As shown here and previously, adaptor-mediated delivery of substrates to AAA+ proteases also involves a progression from low-affinity to high-affinity complexes. This type of assembly has several advantages. From a kinetic perspective, splitting the overall pathway into discrete bimolecular and unimolecular steps speeds assembly. For example, ClpS with bound N-degron substrate could initially dock with any of the six N domains of $ClpA_6$. Moreover, these N domains are highly mobile, further increasing the chances for productive collisions. Subsequent assembly steps would then be unimolecular, allowing the use of relatively weak interactions to position the substrate/adaptor near the translocation machinery of $ClpA_6$.

We propose that adaptors for AAA+ proteases will fall into two general categories. In one category, exemplified by SspB, enzymatic pulling on the substrate disrupts the HADC and initiates degradation. In the second category, exemplified by ClpS, enzymatic tugging on the adaptor destabilizes the HADC, allowing substrate transfer and degradation. Many adaptors that function by a ClpS-type mechanism are likely to be degradation resistant. For example, Rad23 facilitates interactions between ubiquitinated substrates and the proteasome and is refractory to degradation (Heessen et al., 2005; Fishbain et al., 2011). However, a ClpS-type mechanism could also work if the adaptor were degraded. Indeed, the MecA adaptor is degraded by ClpCP during substrate delivery (Turgay et al., 1998).

EXPERIMENTAL PROCEDURES

Proteins and Peptides

Mutants were generated by the QuikChange method (Stratagene) or PCR. ClpS, ClpS mutants, and substrates were initially fused to the C terminus of H_6-Sumo in pET23b (Novagen). Following expression, fusion proteins were purified by Ni-NTA chromatography (QIAGEN) and cleaved with Ulp1 protease. The cleaved H_6-Sumo fragment was removed by passage through Ni-NTA, and the protein of interest was purified by gel filtration on Superdex 75 (GE Healthsciences) and/or ion-exchange chromatography on MonoQ. ClpS variants were concentrated and stored in 20 mM HEPES (pH 7.5), 150 mM KCl, 1 mM DTT, and 10% glycerol. ClpA and ClpP were purified as described (Hou et al., 2008). Trp-$CONH_2$ and Phe-Val (FV) were purchased (Sigma). All remaining peptides were synthesized by standard FMOC techniques using an Apex 396 solid-phase instrument.

Crystallography

Crystals of *E. coli* $ClpS^{26-106}$ were obtained after 3 weeks at 20°C in hanging drops containing 0.5 μl of protein solution (7.5 mg/ml) and 1 μl of reservoir solution (0.2 M ammonium formate, 20% PEG 3350). Crystals were frozen without

additional cryoprotection, and X-ray diffraction data were collected on a Rigaku Micromax 007-HF rotating anode equipped with Varimax-HR mirrors, an RAXIS-IV detector, and an Oxford cryosystem. Data were processed using HKL-2000 (Otwinowski and Minor, 1997). Initial phases were obtained by molecular replacement using PHASER (Storoni et al., 2004) with *E. coli* ClpS 2W9R as a search model. The final structure was obtained by iterative model building using COOT (Emsley and Cowtan, 2004) and refinement using PHENIX (Adams et al., 2002), and had excellent geometry and refinement statistics (Table 1). Rerefinement of the 2W9R, 2WA8, and 2WA9 structures, using COOT and PHENIX, also produced structures with excellent geometry and substantially improved refinement statistics (Table 1).

Fluorescent Labeling

Peptides were labeled with fluorescein maleimide as described (Wang et al., 2008a). ClpS* variants (50 μM) containing a single cysteine were incubated with 50 mM DTT in 100 mM TrisCl (pH 8) for 1.5 hr at 4°C, buffer exchanged into 100 mM Na_2PO_4 (pH 8) and 1 mM EDTA. The ClpS* variants were then singly labeled by addition of 0.3 mg/mL of fluorescein maleimide (Thermo Scientific) for 2 hr at room temperature in the dark. Excess reagent was removed by size-exclusion chromatography, and the modified protein was stored in 10 mM HEPES (pH 7.5), 200 mM KCl, and 1 mM DTT. Binding assays monitored by fluorescence anisotropy were performed using a Photon Technology International Fluorimeter. Data were fitted using a nonlinear squares algorithm to a hyperbolic binding isotherm or to a quadratic equation for tight binding. Reported K_D and K_{app} values are averages ($n \geq 2$) with errors calculated as $SQRT([K\text{-}K_{avg}]^2/n)$.

FeBABE Cleavage

For FeBABE labeling, ^{Q12C}ClpS was incubated in 30 mM MOPS (pH 8.1), 4 mM EDTA at 4°C overnight; desalted into 30 mM MOPS (pH 8.1), 100 mM NaCl, 1 mM EDTA, 5% glycerol; and incubated with 5 μg/μL of Fe(III) (s)-1-(p-bromoacetamidobenzyl)-EDTA (Pierce) for 1 hr at 37°C. FeBABE-ClpS and ClpA were buffer exchanged into 50 mM MOPS (pH 8.1), 300 mM NaCl, 10 mM $MgCl_2$, 10% glycerol; mixed together with no nucleotide or 1 mM ATPγS/ADP; and incubated at room temperature for 30 min. Cleavage was initiated by the addition of 40 mM ascorbate, 10 mM EDTA, followed immediately by 40 mM hydrogen peroxide, 10 mM EDTA. The reaction was quenched by adding SDS-PAGE sample buffer with 40% glycerol and analyzed by SDS-PAGE.

To generate size standards for FeBABE cleavage, Y259C, K265C, and K268C ClpA variants were constructed, purified, incubated with 50 mM DTT at 37°C for ~10 min, and exchanged into 200 mM Tris acetate (pH 8), 1 mM EDTA, 5 M urea, 0.1% SDS. This sample was incubated with 2 mM 2-nitro-5-thiocyanobenzoate at 37°C for 20 min to modify the cysteines and then buffer exchanged into 200 mM Tris acetate (pH 9) and incubated at 45°C for 2 hr to allow protein cleavage.

Degradation and ATPase Assays

ClpAPS degradation assays were performed as described (Wang et al., 2008a). Briefly, $ClpA_6$ (100 nM), $ClpP_{14}$ (200 nM), and ClpS or variants (600 nM) were preincubated in reaction buffer (50 mM HEPES [pH 7.5], 300 mM NaCl, 20 mM $MgCl_2$, 0.5 mM DTT, and 10% glycerol) with substrate for 3 min at 30°C before adding ATP regeneration mix (4 mM ATP, 50 mg/ml creatine kinase, 5 mM creatine phosphate) to initiate degradation. GFP degradation was assayed by loss of fluorescence and the data were fitted by a nonlinear least-squares algorithm to a quadratic version of the Michaelis-Menten equation to obtain K_M and V_{max}. Reported values of kinetic parameters were averages ($n = 3$) ± 1 SD. ATPase rates were monitored under similar conditions but used a coupled ATP-hydrolysis assay (Kim et al., 2000).

ACCESSION NUMBERS

Coordinates for the apo *E. coli* ClpS crystal structure (3O1F) and the rerefined cocrystal structures (3O2B, 3O2H, and 3O2O) have been deposited with the Protein Data Bank.

SUPPLEMENTAL INFORMATION

Supplemental Information includes four figures and can be found with this article online at doi:10.1016/j.molcel.2011.06.009.

ACKNOWLEDGMENTS

We thank S. Bissonnette and P. Chien for helpful discussions and advice, A. de Regt for assistance, and E. Weber-Ban for providing the $^{\Delta L}$ClpA construct. This work was supported by the Howard Hughes Medical Institute (HHMI) and the National Institutes of Health (grants AI-15706, AI-16892, and GM-049224). T.A.B. is an employee of HHMI.

Received: October 7, 2010
Revised: April 10, 2011
Accepted: June 2, 2011
Published: July 21, 2011

REFERENCES

Adams, P.D., Grosse-Kunstleve, R.W., Hung, L.W., Ioerger, T.R., McCoy, A.J., Moriarty, N.W., Read, R.J., Sacchettini, J.C., Sauter, N.K., and Terwilliger, T.C. (2002). PHENIX: building new software for automated crystallographic structure determination. Acta Crystallogr. D Biol. Crystallogr. *58*, 1948–1954.

Bachmair, A., Finley, D., and Varshavsky, A. (1986). In vivo half-life of a protein is a function of its amino-terminal residue. Science *234*, 179–186.

Bolon, D.N., Grant, R.A., Baker, T.A., and Sauer, R.T. (2004). Nucleotide-dependent substrate handoff from the SspB adaptor to the AAA+ ClpXP protease. Mol. Cell *16*, 343–350.

Burton, R.E., Siddiqui, S.M., Kim, Y.I., Baker, T.A., and Sauer, R.T. (2001). Effects of protein stability and structure on substrate processing by the ClpXP unfolding and degradation machine. EMBO J. *20*, 3092–3100.

Burton, B.M., and Baker, T.A. (2005). Remodeling protein complexes: insights from the AAA+ unfoldase ClpX and Mu transposase. Protein Sci. *14*, 1945–1954.

Cranz-Mileva, S., Imkamp, F., Kolygo, K., Maglica, Z., Kress, W., and Weber-Ban, E. (2008). The flexible attachment of the N-domains to the ClpA ring body allows their use on demand. J. Mol. Biol. *378*, 412–424.

Davis, I.W., Leaver-Fay, A., Chen, V.B., Block, J.N., Kapral, G.J., Wang, X., Murray, L.W., Arendall, W.B., Snoeyink, J., Richardson, J.S., and Richardson, D.C. (2007). MolProbity: all-atom contacts and structure validation for proteins and nucleic acids. Nucleic Acids Res. *35*, W375–W383.

De Donatis, G.M., Singh, S.K., Viswanathan, S., and Maurizi, M.R. (2010). A single ClpS monomer is sufficient to direct the activity of the ClpA hexamer. J. Biol. Chem. *285*, 8771–8781.

Dougan, D.A., Reid, B.G., Horwich, A.L., and Bukau, B. (2002). ClpS, a substrate modulator of the ClpAP machine. Mol. Cell *9*, 673–683.

Dougan, D.A., Truscott, K.N., and Zeth, K. (2010). The bacterial N-end rule pathway: expect the unexpected. Mol. Microbiol. *76*, 545–558.

Effantin, G., Ishikawa, T., De Donatis, G.M., Maurizi, M.R., and Steven, A.C. (2010). Local and global mobility in the ClpA AAA+ chaperone detected by cryo-electron microscopy: functional connotations. Structure *18*, 553–562.

Emsley, P., and Cowtan, K. (2004). Coot: model-building tools for molecular graphics. Acta Crystallogr. D Biol. Crystallogr. *60*, 2126–2132.

Erbse, A., Schmidt, R., Bornemann, T., Schneider-Mergener, J., Mogk, A., Zahn, R., Dougan, D.A., and Bukau, B. (2006). ClpS is an essential component of the N-end rule pathway in *Escherichia coli*. Nature *439*, 753–756.

Fishbain, S., Prakash, S., Herrig, A., Elasser, S., and Matouschek, A. (2011). Rad23 escapes degradation because it lacks a proteasome initiation region. Nat. Commun. *2*, 192.

Gottesman, S., and Maurizi, M.R. (1992). Regulation by proteolysis: energy-dependent proteases and their targets. Microbiol. Rev. *56*, 592–621.

Guo, F., Maurizi, M.R., Esser, L., and Xia, D. (2002). Crystal structure of ClpA, an Hsp100 chaperone and regulator of ClpAP protease. J. Biol. Chem. *277*, 46743–46752.

Heessen, S., Masucci, M.G., and Dantuma, N.P. (2005). The UBA2 domain functions as an intrinsic stabilization signal that protects Rad23 from proteasomal degradation. Mol. Cell *18*, 225–235.

Hinnerwisch, J., Fenton, W.A., Furtak, K.J., Farr, G.W., and Horwich, A.L. (2005). Loops in the central channel of ClpA chaperone mediate protein binding, unfolding, and translocation. Cell *121*, 1029–1041.

Hou, J.Y., Sauer, R.T., and Baker, T.A. (2008). Distinct structural elements of the adaptor ClpS are required for regulating degradation by ClpAP. Nat. Struct. Mol. Biol. *15*, 288–294.

Kenniston, J.A., Baker, T.A., Fernandez, J.M., and Sauer, R.T. (2003). Linkage between ATP consumption and mechanical unfolding during the protein processing reactions of an AAA+ degradation machine. Cell *114*, 511–520.

Kenniston, J.A., Baker, T.A., and Sauer, R.T. (2005). Partitioning between unfolding and release of native domains during ClpXP degradation determines substrate selectivity and partial processing. Proc. Natl. Acad. Sci. USA *102*, 1390–1395.

Kim, Y.I., Burton, R.E., Burton, B.M., Sauer, R.T., and Baker, T.A. (2000). Dynamics of substrate denaturation and translocation by the ClpXP degradation machine. Mol. Cell *5*, 639–648.

Koodathingal, P., Jaffe, N.E., Kraut, D.A., Prakash, S., Fishbain, S., Herman, C., and Matouschek, A. (2009). ATP-dependent proteases differ substantially in their ability to unfold globular proteins. J. Biol. Chem. *284*, 18674–18684.

Kress, W., Mutschler, H., and Weber-Ban, E. (2009). Both ATPase domains of ClpA are critical for processing of stable protein structures. J. Biol. Chem. *284*, 31441–31452.

Lee, C., Schwartz, M.P., Prakash, S., Iwakura, M., and Matouschek, A. (2001). ATP-dependent proteases degrade their substrates by processively unraveling them from the degradation signal. Mol. Cell *7*, 627–637.

Levchenko, I., Seidel, M., Sauer, R.T., and Baker, T.A. (2000). A specificity-enhancing factor for the ClpXP degradation machine. Science *289*, 2354–2356.

Levchenko, I., Grant, R.A., Wah, D.A., Sauer, R.T., and Baker, T.A. (2003). Structure of a delivery protein for a AAA+ protease in complex with a peptide degradation tag. Mol. Cell *12*, 365–372.

Lupas, A.N., and Koretke, K.K. (2003). Bioinformatic analysis of ClpS, a protein module involved in prokaryotic and eukaryotic protein degradation. J. Struct. Biol. *141*, 77–83.

Martin, A., Baker, T.A., and Sauer, R.T. (2008). Diverse pore loops of the AAA+ ClpX machine mediate unassisted and adaptor-dependent recognition of ssrA-tagged substrates. Mol. Cell *29*, 441–450.

Otwinowski, Z., and Minor, W. (1997). Processing of X-ray diffraction data collected in oscillation mode. In Methods in Enzymology, Volume 276: Macromolecular Crystallography, A, C.W. Carter, Jr. and R.M. Sweet, eds. (New York: Academic Press), pp. 307–326.

Román-Hernández, G., Grant, R.A., Sauer, R.T., and Baker, T.A. (2009). Molecular basis of substrate selection by the N-end rule adaptor protein ClpS. Proc. Natl. Acad. Sci. USA *106*, 8888–8893.

Schuenemann, V.J., Kralik, S.M., Albrecht, R., Spall, S.K., Truscott, K.N., Dougan, D.A., and Zeth, K. (2009). Structural basis of N-end rule substrate recognition in *Escherichia coli* by the ClpAP adaptor protein ClpS. EMBO Rep. *10*, 508–514.

Storoni, L.C., McCoy, A.J., and Read, R.J. (2004). Likelihood-enhanced fast rotation functions. Acta Crystallogr. D Biol. Crystallogr. *60*, 432–438.

Striebel, F., Kress, W., and Weber-Ban, E. (2009). Controlled destruction: AAA+ ATPases in protein degradation from bacteria to eukaryotes. Curr. Opin. Struct. Biol. *19*, 209–217.

Tasaki, T., and Kwon, Y.T. (2007). The mammalian N-end rule pathway: new insights into its components and physiological roles. Trends Biochem. Sci. *32*, 520–528.

Tobias, J.W., Shrader, T.E., Rocap, G., and Varshavsky, A. (1991). The N-end rule in bacteria. Science *254*, 1374–1377.

Turgay, K., Hahn, J., Burghoorn, J., and Dubnau, D. (1998). Competence in *Bacillus subtilis* is controlled by regulated proteolysis of a transcription factor. EMBO J. *17*, 6730–6738.

Varshavsky, A. (2008). Discovery of cellular regulation by protein degradation. J. Biol. Chem. *283*, 34469–34489.

Wah, D.A., Levchenko, I., Rieckhof, G.E., Bolon, D.N., Baker, T.A., and Sauer, R.T. (2003). Flexible linkers leash the substrate-binding domain of SspB to a peptide module that stabilizes delivery complexes with the AAA+ ClpXP protease. Mol. Cell *12*, 355–363.

Wang, K.H., Sauer, R.T., and Baker, T.A. (2007). ClpS modulates but is not essential for bacterial N-end rule degradation. Genes Dev. *21*, 403–408.

Wang, K.H., Román-Hernández, G., Grant, R.A., Sauer, R.T., and Baker, T.A. (2008a). The molecular basis of N-end rule recognition. Mol. Cell *32*, 406–414.

Wang, K.H., Oakes, E.S.C., Sauer, R.T., and Baker, T.A. (2008b). Tuning the strength of a bacterial N-end rule degradation signal. J. Biol. Chem. *283*, 24600–24607.

Weber-Ban, E.U., Reid, B.G., Miranker, A.D., and Horwich, A.L. (1999). Global unfolding of a substrate protein by the Hsp100 chaperone ClpA. Nature *401*, 90–93.

Wolfgang, K., and Weber-Ban, E. (2009). The alternating power stroke of a 6-cylinder AAA protease chaperone engine. Mol. Cell *35*, 574–585.

Word, J.M., Lovell, S.C., Richardson, J.S., and Richardson, D.C. (1999). Asparagine and glutamine: using hydrogen atom contacts in the choice of side-chain amide orientation. J. Mol. Biol. *285*, 1735–1747.

Xia, D., Esser, L., Singh, S.K., Guo, F., and Maurizi, M.R. (2004). Crystallographic investigation of peptide binding sites in the N-domain of the ClpA chaperone. J. Struct. Biol. *146*, 166–179.

Zeth, K., Ravelli, R.B., Paal, K., Cusack, S., Bukau, B., and Dougan, D.A. (2002). Structural analysis of the adaptor protein ClpS in complex with the N-terminal domain of ClpA. Nat. Struct. Biol. *9*, 906–911.